Magnetoresistance and Kondo effect in the nodal-line semimetal VAs_2

Shuijin Chen,[1] Zhefeng Lou,[1] Qin Chen,[1] Binjie Xu,[1] Chunxiang Wu,[1]
Jianhua Du,[2] Jinhu Yang,[3] Hangdong Wang,[3] and Minghu Fang[1,4,*]

[1] *Department of Physics, Zhejiang University, Hangzhou* 310027, *China*
[2] *Department of Applied Physics, China Jiliang University, Hangzhou* 310018, *China*
[3] *Department of Physics, Hangzhou Normal University, Hangzhou* 310036, *China*
[4] *Collaborative Innovation Center of Advanced Microstructures, Nanjing University, Nanjing* 210093, *China*

(Dated: March 1, 2022)

We performed calculations of the electronic band structure and the Fermi surface as well as measured the longitudinal resistivity $\rho_{xx}(T,H)$, Hall resistivity $\rho_{xy}(T,H)$, and magnetic susceptibility as a function of temperature and various magnetic fields for VAs_2 with a monoclinic crystal structure. The band structure calculations show that VAs_2 is a nodal-line semimetal when spin-orbit coupling is ignored. The emergence of a minimum at around 11 K in $\rho_{xx}(T)$ measured at $H = 0$ demonstrates that an additional magnetic impurity (V^{4+}, $S = 1/2$) occurs in VAs_2 single crystals, evidenced by both the fitting of $\rho_{xx}(T)$ data and the susceptibility measurements. It was found that a large positive magnetoresistance (MR) reaching 649% at 10 K and 9 T, its nearly quadratic field dependence, and a field-induced up-turn behavior of $\rho_{xx}(T)$ emerge also in VAs_2, although MR is not so large due to the existence of additional scattering compared with other topological nontrival/trival semimetals. The observed properties are attributed to a perfect charge-carrier compensation, which is evidenced by both calculations relying on the Fermi surface and the Hall resistivity measurements. These results indicate that the compounds containing V ($3d^34s^2$) element as a platform for studying the influence of magnetic impurities to the topological properties.

arXiv:2012.11997v1 [cond-mat.str-el] 22 Dec 2020

Since the discovery of quantum Hall effect in the two-dimensional electron gas in the 1980s [1], it has been recognized that the topology of band structure in the solid materials plays an important role in the classification of maters and the understanding of physical properties. Then, many topological materials, such as, topological insulators [2–4], Dirac semimetals [5, 6], Weyl semimetals [7–9] and nodal-line semimetals [10–13] have been proposed theoretically and confirmed experimentally. Most of them are free of strong correlation effects. In the presence of strong electron interactions, very fruitful topological phases can be expected, such as the topological Mott [14] or Kondo insulators [15–17], topological superconductors [18], and fractional topological insulators [19–21]. In order to pursue these exotic phases, searching for suitable compounds, which are strongly correlated (usually in d and f orbital systems) and topologically nontrivial, attracts much attention. For instance, SmB_6, as a typical rare-earth mixed valence compound, in which, has been proposed theoretically as a topological Kondo insulator [15–17] and recently has been confirmed by transport [22–25], photoemission [26–28] and scanning tunneling microscope (STM) [29] experiments. At sufficiently low temperature, the hybridization between $4f$ orbitals and highly dispersive $5d$ bands results in the formation of "heavy fermion" bands, thus, SmB_6 is a correlated $\mathcal{Z}_2$ topological insulator. Recently, a number of groups [30–33] predicted thousands of candidate topological materials by performing systematic high-throughput computational screening across the databases of known materials. Following these predictions, it is possible to search for the topological materials in the known compounds containing $3d$ elements based on the calculations of band structure, and the measurements of physical properties.

VAs_2 crystalizes in a monoclinic structure with space group $C_{12/m1}$ (No. 12), as shown in Fig. 1(a), has an isostructure to the transition metal dipnictides XPn_2 (X = Nb, Ta; Pn = P, As, Sb) [34–40], which have been widely studied theoretically and experimentally as a class of topological materials. For example, Baokai Wang *et al*. [41] identified the presence of a rotational-symmetry-protected topological crystalline insulator (TCI) states in these compounds based on first-principles calculations combined with a symmetry analysis. It was found that all these compounds exhibit high mobilities and extremely large positive MR [35–40]. Interestingly, a negative longitudinal MR when the applied field is parallel to the current direction was observed in both $TaSb_2$ [38] and $TaAs_2$ [40], similar to that observed in the known weyl semimetals TaAs family [7–9, 42–47]. Compared to the $4d/5d$ electrons in $NbAs_2/TaAs_2$, the more localization of the $3d$ electrons in VAs_2 might lead to a stronger electronic correlation, or introduce an additional magnetic scattering to the carriers (Kondo effect).

In this paper, we grew successfully VAs_2 crystals with a monoclinic structure and measured its longitudinal resistivity $\rho_{xx}(T,H)$, Hall resistivity $\rho_{xy}(T,H)$, and magnetic susceptibility as a function of temperature at various magnetic fields, as well as calculated its electronic band structure and Fermi surface (FS). The band structure calculations show that VAs_2 is also a nodal-line semimetal when spin-orbit coupling (SOC) is ignored. It was found that the $\rho_{xx}(T)$ measured at $H = 0$ exhibits a minimum at around 11 K, which is considered of originate from the magnetic impurities V^{4+} ($S = 1/2$) scattering (*i.e.* Kondo effect) , evidenced by both the susceptibility measurements and the fitting of $\rho_{xx}(T)$ data at low temperatures. We further reveal a nearly quadratic field dependence of MR, reaching 649% at 10 K and 9 T, a field-induced up-turn behavior of $\rho_{xx}(T)$ in this material, which are attributed to a perfect charge-carrier compensation, evidenced by both the calculations relying on the FS topology and the Hall resistivity measurements.

VAs_2 single crystals were grown by a chemical vapor transport method. High purity V and As powder were mixed in a mole ratio 1 : 2, then sealed in an evacuated silica tube containing I_2 as a transport agent with 10 mg/cm^3. The quartz tube was placed in a tube furnace with a temperature gradient of 950°C - 750°C and heated for two weeks. Polyhedral crystals were obtained at the cold end of the tube. A single crystal with a dimension of $2.0 \times 0.73 \times 0.29$ mm^3 [see Fig. 1(b)] and a cleavage surface (001) was selected for the transport and magnetic property measurements. The composition was detected to be V : As = 32.7 : 67, using the Energy Dispersive X-ray Spectrometer (EDXS), the crystal structure was determined by the single-crystal X-Ray diffraction, as shown in Fig. 1(c), from which, the lattice parameter, $c = 7.481(7)$ Å, consistent with the result in Ref. [48]. The longitudinal resistivity and Hall resistivity measurements were carried out on a physical property measurement system (Quantum Design, PPMS-9 T) with a standard four-probe method [see Fig. 1(b)]. The magnetization measurements were carried out on a magnetic property measurement system (Quantum Design, MPMS-7 T). The band structure was calculated by using the Vienna *ab initio* simulation package (VASP) [49, 50] with a generalized gradient approximation (GGA) of Perdew, Burke and Ernzerhof (PBE) [51] for the exchange correlation potential. A cutoff energy of 520 eV and a $10 \times 10 \times 6$ k-point mesh were used to perform the bulk calculations. The nodal-line search and FS calculations were performed by using the open-source software WannierTools [52] that is based on the Wannier tight-binding model (WTBM) constructed using Wannier90 [53].

First at all, we discuss the results of our electronic structure calculations that extend the initial prediction of the high symmetry line semimetal for VAs_2 [32]. In order to address the topological character of VAs_2, we calculate its band structure and the FS. As shown in Fig. 1(d), there are six different FS sheets: two hole-like surfaces (green) at the L and Y points, and four electron-like (red) surfaces near L and Z points, the volume of the electron and hole pockets is roughly the same, indicating that VAs_2 is nearly an electron-hole compensated semimetal, also evidenced by the Hall resistivity measurements discussed as follows. The bulk band structure of VAs_2 without and with SOC is presented in Fig. 1(f) and 1(g), respectively. It can be seen clearly that the bands near the Fermi level mainly arise from the d orbits of V atoms, and the valence and conduction bands cross along the Y-X_1, Z-I_1 and L-I high symmetry directions. Without SOC, in the Brillouin zones (BZ), the nodal lines can be found by using the open-source software WannierTool [52], see in Fig. 1(h). There are two type of nodal lines, one is two nonclosed spiral lines extending across the BZ through point Z, another is two nodal loops near the L point. When SOC is included, these nodal lines are gapped [see Fig. 1(g)] and lead to a band inversion along the Y-X_1, Z-I_1 and L-I high symmetry directions, driving into a topological crystalline insulator (TCI), as discussed by Baokai Wang *et al*. [41] for the identical structure transition metal dipnitides RX_2 (R = Nb or Ta; X = P, As or Sb). Although the opening of a local band gap between the valence and conduction bands occurs when SOC is included, VAs_2 preserves its semimetal character with the presence of electron and hole pockets, similar to that in $NbAs_2$ reported in Ref. [41].

Next, we focus on the Kondo effect emerging in the longitudinal resistivity for VAs_2. Figure 2(a) shows the temperature dependence of resistivity, $\rho_{xx}(T)$. With decreasing temperature, the resistivity, ρ_{xx}, decreases monotonously from $\rho_{xx}(300\text{ K}) = 78$ $\mu\Omega$ cm, reaches a minimum at around 11 K, then increases a little to 6.4 $\mu\Omega$ cm at 2 K, thus the residual resistivity ratio (RRR) $\rho_{xx}(300\text{ K})/\rho_{xx}$ (2 K) ~ 12, much smaller than that observed in the other transition metal dipnictide crystals, such as $NbAs_2$ ($\sim$ 75) [37], $TaAs_2$ ($\sim$ 100) [40]. As we know, the system, containing magnetic impurities which usually scatter the conduction electrons through the $s-d$ exchange interactions, exhibits a minimum in resistivity at lower temperatures, *i.e.* termed as the Kondo effect [54, 55]. As discussed by S. Barua *et al*. for VSe_2 [56], considering the correction to the resistivity due to the Ruderman-Kittel-Kasuya-Yosida (RKKY) interactions between the paramagnetic V^{4+} ions, the Kondo resistivity described by the Hamann expression is modified to:

$$\rho_{sd} = \frac{\rho_0}{2}\left[1 - \frac{\ln(T_{eff}/T_K)}{\left[\ln^2(T_{eff}/T_K) + S(S+1)\pi^2\right]^{1/2}}\right] \quad (1)$$

where ρ_0 is the unitarity limit, T_K is the Kondo temperature and S is the spin of magnetic impurity, the effective temperature $T_{eff} = (T^2 + T_W^2)^{1/2}$, in which $k_B T_W$ is the effective RKKY interaction strength [54], replaces to T in the original expression [56]. The temperature dependence of resistivity, $\rho_{xx}(T)$, is expressed as :

$$\rho(T) = \rho_{sd} + bT^2 + cT^5 + \rho_b \quad (2)$$

where bT^n term is the electron-phonon scattering contribution, ρ_b is an independent resistivity. We used Eq. (2) to fit the resistivity data measured at low temperatures (2 - 40 K). The results are shown in the inset in Fig. 2(a), it is clear that Eq. (2) can well describe the $\rho(T)$ data below 40 K, and the obtained parameters in Eq. (1) and Eq. (2) from the fitting are listed in TABLE I. The existence of V^{4+} ($S = 1/2$) impurities in our VAs_2 crystal was

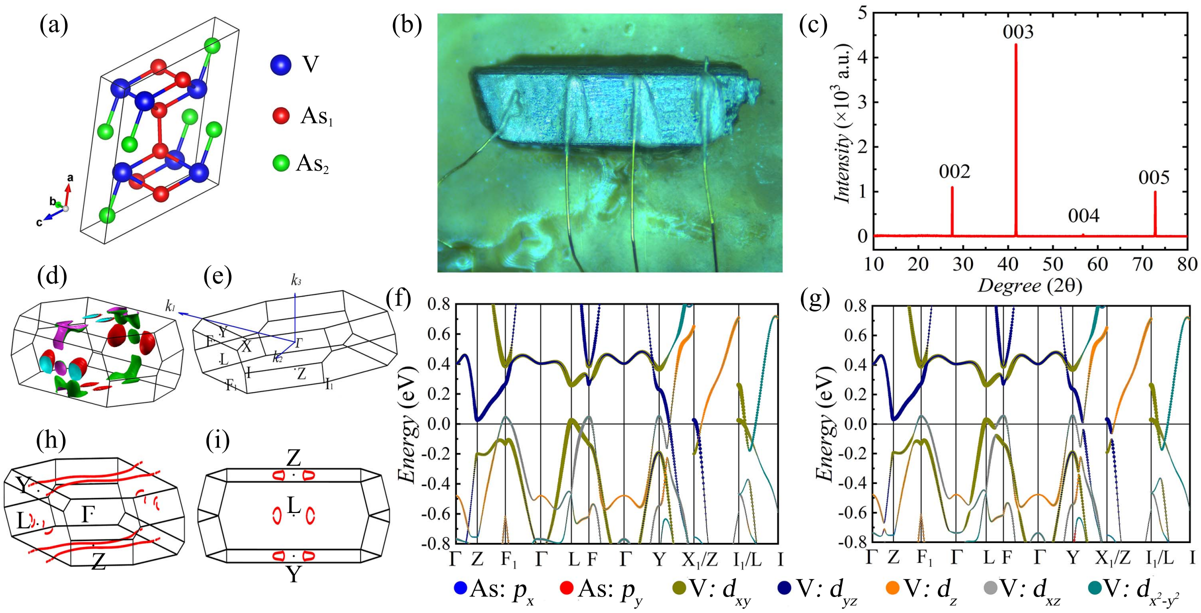

Figure 1. (a) Crystal structure of VAs_2. (b) Photograph of a VAs_2 crystal with 4 wires for resistance measurements. (c) Single crystal XRD pattern of VAs_2. (d) The calculated Fermi surface of VAs_2. (e) The Brillouin zone. (f) and (g) Band structures calculated without and with considering SOC. (h) and (i) Nodal lines in the first Brillouin zone from different perspective.

TABLE I. The obtained parameters by the fitting to $\rho(T)$ data using Eq. (2).

ρ_0 ($\mu\Omega$ cm)	ρ_b ($\mu\Omega$ cm)	b ($\mu\Omega$ cm/K^2)	c ($\mu\Omega$ cm/K^5)	T_K (K)	T_W (K)	S
2.33	4.7	1.3×10^{-3}	1.0×10^{-9}	7.23	0.78	0.5

confirmed by the magnetic susceptibility measurements. The temperature dependence of magnetic susceptibility, $\chi(T)$, measured at 1 T with a field-cooling (FC) process is presented in Fig. 2(b). With decreasing temperature, the susceptibility χ decreases a little, reaches a minimum at around 180 K, then increases strikingly below 100 K. No magnetic transition was observed in the whole temperature range (2 - 300 K), and the significant increase of χ in the lower temperatures was considered to originate from the contribution of V^{4+} ($S = 1/2$) impurities existing in crystal as the interstitial ions, as observed in VSe_2 crystals [56]. We used the Curie-Weiss law $\chi = \frac{C}{T-\theta}$, to fit the data below 40 K, as shown in Fig. 2(a), the Curie constant $C = 1.27$ (±0.02)$\times10^{-3}$ emu K/mol, and the curie temperature θ = -2.61 ($\pm$0.08) K, were obtained. The nearly linear relationship between $1/\chi$ and T below 40 K [see the inset in Fig. 2(b)] demonstrates the reliability of the fitting. The V^{4+} ($S = 1/2$) impurity molar fraction was estimated to be of 0.34 ($\pm$0.02) %, small amount impurities existing in the crystals.

Third, we discuss the magnetoresisitance (MR) occurring in the nodal-line semimetal VAs_2, with the presence of Kondo scattering of V^{4+}. Figure 3(a) presents the temperature dependence of longitudinal resistivity, $\rho_{xx}(T)$, measured at various magnetic fields H, with current I applied in the (001) plane, and $H \perp$ (001) plane. Similar to many other nontrivial and trivial topological semimetals [35, 36, 38], VAs_2 also exhibits a large MR. As shown in Fig. 3(a), an up-turn in ρ_{xx}(T) curves under applied magnetic field occurs at low temperatures: ρ_{xx} increases with decreasing T and then saturates. Figure 3(b) shows MR as a function of temperature measured at various magnetic fields, with the conventional definition $MR=\frac{\Delta\rho}{\rho(0)}=[\frac{\rho(H)-\rho(0)}{\rho(0)}] \times 100\%$. The normalized MR, shown in the inset of Fig. 3(b), has the same temperature dependence for various fields, excluding the suggestion of a field-induced metal-insulator transition [57, 58] at low temperatures, as discussed in our works addressing the topological trivial semimetal α-WP_2 [59], for the nodal-line semimetal MoO_2 [13], and the work of Thoutam *et al.* on the type-II weyl semimetal WTe_2 [60]. Figure 3(c) displays $\rho_{xx}(T)$, measured at 0 and 9 T, as well as their difference $\Delta\rho_{xx} = \rho_{xx}(T$, 9 T) - $\rho_{xx}(T$, 0 T). It is clear that the resistivity in a applied magnetic field consists of two components, $\rho_0(T)$ and $\Delta\rho_{xx}$, with opposite temperature dependencies. As discussed by us for α-WP_2 [59], MoO_2 [13] and by Thoutam *et al.* for

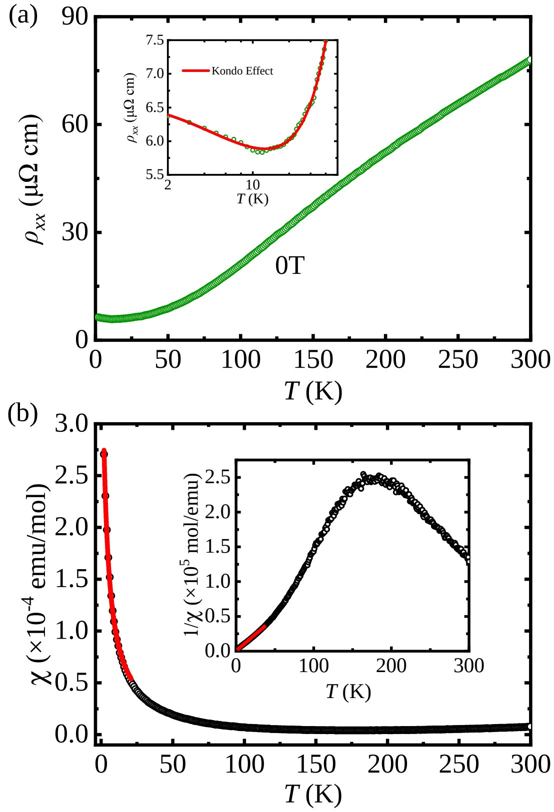

Figure 2. (a) Temperature dependence of resistivity $\rho(T)$, inset: the $\rho(T)$ data below 40 K and the fitting by Eq. (2). (b) magnetic susceptibility, measured at 1 T, inset: $1/\chi(T)$.

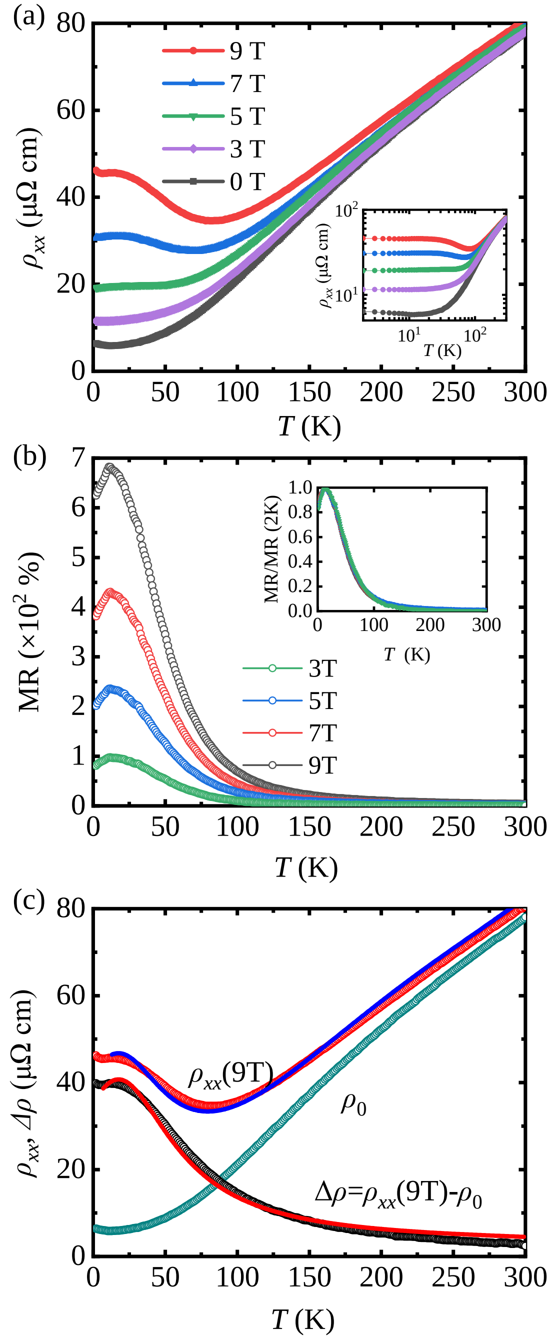

Figure 3. (Color online) (a) Temperature dependence of resistivity measured at various magnetic fields. (b) The MR vs. temperature under various magnetic fields. The inset is normalized MR. (c) Temperature dependence of resistivity at 0 and 9 T and their difference. The red and blue lines are the fitting lines using the Kohler scaling law.

WTe_2 [60], the resistivity can be written as :

$$\rho_{xx}(T,H) = \rho_0(T)[1 + \alpha(H/\rho_0)^m] \tag{3}$$

The second term is the magnetic-field-induced resistivity $\Delta\rho_{xx}$, which follows the Kohler rule with two constants α and m. $\Delta\rho_{xx}$ is proportional to $1/\rho_0$ (when $m = 2$) and competes with the first term upon changing temperature, possibly giving rise to a minimum in $\rho(T)$ curves. Figure 4(a) presents MR as a function of field at various temperatures. The measured MR is large at low temperatures, reaching 649 % at 10 K and 9 T, and does not show any of saturation up to the highest field (9 T) in our measurements. As discussed above, MR can be described by the Kohler scaling law [61, 62]:

$$MR = \frac{\Delta\rho_{xx}(T,H)}{\rho_0(T)} = \alpha(H/\rho_0)^m \tag{4}$$

As shown in Fig. 4(b), all MR data from 2 - 100 K collapse onto a single straight line in the plotted as $MR \sim H/\rho_0$ curve, and $\alpha = 0.038$ $(\mu\Omega\ \mathrm{cm/T})^{1.76}$ and $m = 1.76$ were obtained by fitting. The nearly quadratic field dependence of MR observed in this nodal-line semimetal

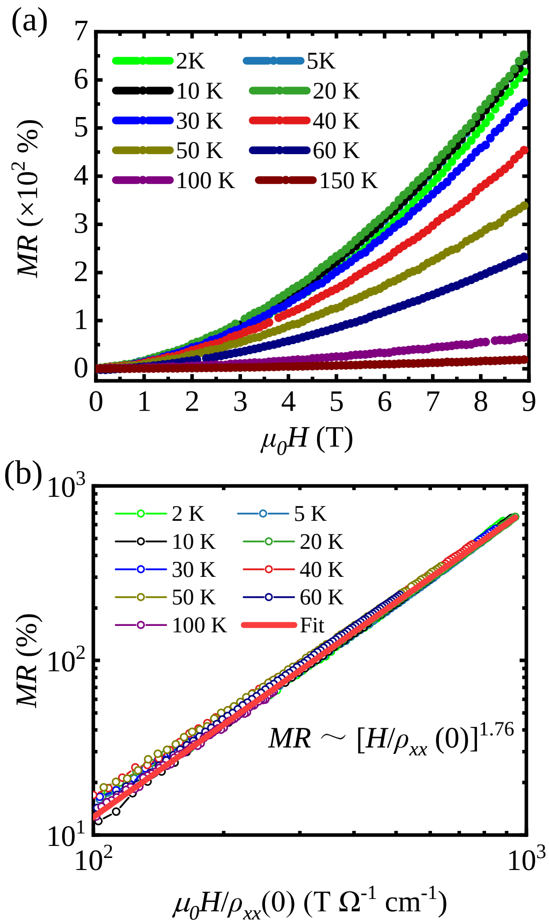

Figure 4. (a) Field dependence of MR at various temperature. (b) MR plotted as a log scale as a function of $H/\rho_{xx}(0)$.

VAs_2 is attributed to the electron-hole compensation, evidenced by FS calculations mentioned above, as well as the Hall resistivity measurements discussed below, which is a common characteristics for the most topologically nontrivial and trivial semimetals [35, 36, 38]. Figure 5(a) displays the Hall resistivity, $\rho_{xy}(H)$, measured at various temperatures for a VAs_2 crystal with $H \parallel c$ axis. The nonlinear field dependence of $\rho_{xy}(H)$ below 100 K demonstrates its semimetal characteristics, in which both electron and hole carriers coexist. Following the analysis of Ref. [63] for $\gamma-MoTe_2$ [64] and by us for MoO_2 [13], we analyze the longitudinal and Hall resistivity by using the two-carrier model. In this model, the conductivity tensor, in its complex representation, is giving by [65]:

$$\sigma = \frac{en_e\mu_e}{1 + i\mu_e\mu_0 H} + \frac{en_h\mu_h}{1 + i\mu_h\mu_0 H} \tag{5}$$

where n_e (n_h) and μ_e (μ_h) denote the carrier concentrations and mobilities of electrons (holes), respectively. To appropriately evaluate the carrier densities and mobilities, we calculated the Hall conductivity $\sigma_{xy} = -\frac{\rho_{xy}}{\rho_{xx}^2+\rho_{xy}^2}$ and the longitudinal conductivity $\sigma_{xx} = \frac{\rho_{xx}}{\rho_{xx}^2+\rho_{xy}^2}$ by using the original experimental $\rho_{xy}(H)$ and $\rho_{xx}(H)$ data. Then, we fit both $\sigma_{xy}(H)$ and $\sigma_{xx}(H)$ data by using the same fitting parameters and the field dependence given by [64]:

$$\sigma_{xy} = \frac{e(\mu_0 H)n_h\mu_h^2}{1 + \mu_h^2(\mu_0 H)^2} - \frac{e(\mu_0 H)n_e\mu_e^2}{1 + \mu_e^2(\mu_0 H)^2} \tag{6}$$

$$\sigma_{xx} = \frac{en_h\mu_h}{1 + \mu_h^2(\mu_0 H)^2} + \frac{en_e\mu_e}{1 + \mu_e^2(\mu_0 H)^2} \tag{7}$$

Figures 5(c) and 5(d) display the fitting of both the $\sigma_{xy}(H)$ and $\sigma_{xx}(H)$ measured at T = 2 - 60 K, respectively. The excellent agreement between our experimental data and the two-carrier model over a broad range of temperature, confirms the coexistence of electrons and holes in VAs_2. Figure 5(b) shows the obtained n_e, n_h, μ_e and μ_h values by fittings as a function of temperature. The almost same values of n_e and n_h below 60 K [see the inset Fig. 5(b)], such as n_e = 1.77 $\times 10^{20}$ cm^{-3} and n_h = 1.69 $\times 10^{20}$ cm^{-3} at 2 K, indicate that VAs_2 is indeed a electron-hole compensated semimetal, consistent with the above results from the calculation FS. Both electron and hole densities are estimated to be 10^{20} cm^{-3} in our VAs_2 crystal, significantly higher than those in Dirac semimetals, such as, Cd_3As_2 ($\sim 10^{18}$ cm^{-3} [66]) and Na_3Bi ($\sim 10^{17}$ cm^{-3} [67]), but comparable to these of another nodal-line semimetals ZrSiS ($\sim 10^{20}$ cm^{-3} [11]), and MoO_2 ($\sim 10^{20}$ cm^{-3} [13]), demonstrating further the nodal-line characteristics of VAs_2. As shown in Fig. 5(b), it is clear that the hole mobility μ_h is higher than μ_e in the whole temperature range (2 - 300 K), such as, at 2 K, μ_h = 4.08 $\times 10^3$ cm^2/Vs, μ_e = 1.54 $\times 10^3$ cm^2/Vs, but smaller one order of magnitude than these observed by us in the nodal-line semimetal MoO_2 ($\sim 10^4$ cm^2/Vs) [13], and both μ_h and μ_e decrease notably with increasing temperature due to the existence of phonon thermal scattering at higher temperatures. It is worth noting that both μ_h and μ_e have a little decrease below 11 K, corresponding to the Kondo scattering from V^{4+} magnetic impurities mentioned above.

In summary, we calculated the electronic structure, and measured the longitudinal resistivity, Hall resistivity and magnetic susceptibility for VAs_2. It was found that VAs_2 exhibits many common characteristics of the topological nontrivial/trivial semimetals, such as a large MR reaching 649% at 10 K and 9 T, a nearly quadratic field dependence of MR, and a field-induced up-turn behaviour in $\rho_{xx}(T)$. Both the FS calculations and the Hall resistivity measurements verify these properties being attributed to a perfect carrier compensation. Interestingly, the Kondo scattering due to the existence of V^{4+} (S = 1/2) magnetic impurities in our VAs_2 crystals occurs,

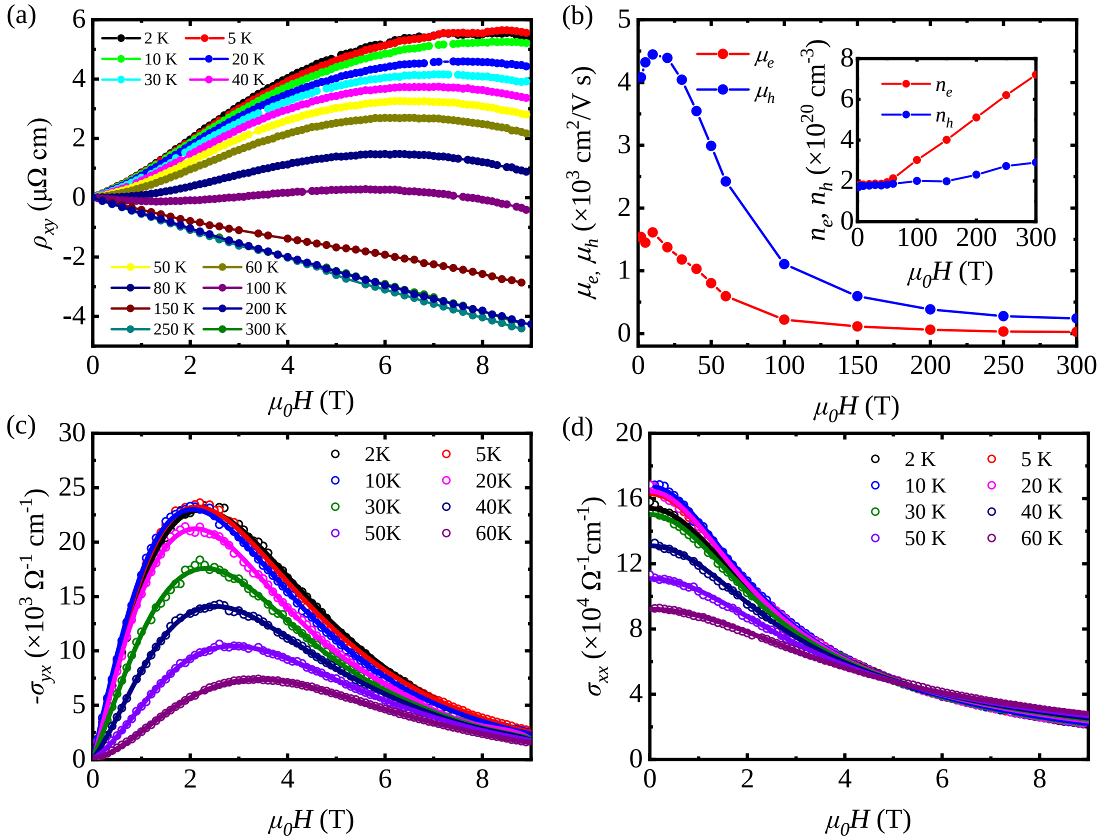

Figure 5. (a) Field dependence of Hall resistivity ρ_{xy} measured at various temperatures for VAs_2 crystal. (b) Charge-carrier mobilities μ_e and μ_h, and (inset) the carrier concentrations, n_e and n_h, as a function of temperature extracted from the two-carrier model analysis of both σ_{xy} and σ_{xx} data. Components of the conductivity tenser, *i.e.* σ_{xy} and σ_{xx} in the panels (c) and (d), respectively, as a function of magnetic field for different temperatures (< 60 K). Hollow dots represent experimental data and solid lines are the fitting curves by using the two-carrier model.

indicating that VAs_2 crystal can be used to study the Kondo effect in the nodal-line semimetal.

ACKNOWLEDGEMENTS: This research is supported by the Ministry of Science and Technology of China under Grant No. 2016YFA0300402 and the National Natural Science Foundation of China (NSFC) (NSFC-12074335 and No. 11974095), the Zhejiang Natural Science Foundation (No. LY16A040012) and the Fundamental Research Funds for the Central Universities.

* Corresponding author: mhfang@zju.edu.cn

[1] R. B. Laughlin, Phys. Rev. Lett. **50**, 1395 (1983).
[2] C. L. Kane and E. J. Mele, Phys. Rev. Lett. **95**, 226801 (2005).
[3] B. A. Bernevig and S.-C. Zhang, Phys. Rev. Lett. **96**, 106802 (2006).
[4] L. Fu, Phys. Rev. Lett. **103**, 266801 (2009).
[5] Z. Liu, B. Zhou, Y. Zhang, Z. Wang, H. Weng, D. Prabhakaran, S.-K. Mo, Z. Shen, Z. Fang, X. Dai, Z. Hussain, and Y. Chen, Science (New York, N.Y.) **343**, 864 (2014).
[6] Z. Wang, H. Weng, Q. Wu, X. Dai, and Z. Fang, Phys. Rev. B **88**, 125427 (2013).
[7] C. Shekhar, A. K. Nayak, Y. Sun, M. Schmidt, M. Nicklas, I. Leermakers, U. Zeitler, Y. Skourski, J. Wosnitza, Z. Liu, *et al.*, Nature Physics **11**, 645 (2015).
[8] B. Q. Lv, H. M. Weng, B. B. Fu, X. P. Wang, H. Miao, J. Ma, P. Richard, X. C. Huang, L. X. Zhao, G. F. Chen, Z. Fang, X. Dai, T. Qian, and H. Ding, Phys. Rev. X **5**, 031013 (2015).
[9] J. Du, H. Wang, Q. Chen, Q. Mao, R. Khan, B. Xu, Y. Zhou, Y. Zhang, J. Yang, B. Chen, *et al.*, Science China Physics, Mechanics & Astronomy **59**, 657406 (2016).
[10] L. An, X. Zhu, W. Gao, M. Wu, W. Ning, and M. Tian, Phys. Rev. B **99**, 045143 (2019).
[11] J. Hu, Z. Tang, J. Liu, X. Liu, Y. Zhu, D. Graf, K. Myhro, S. Tran, C. N. Lau, J. Wei, and Z. Mao, Phys. Rev. Lett. **117**, 016602 (2016).

[12] E. Emmanouilidou, B. Shen, X. Deng, T.-R. Chang, A. Shi, G. Kotliar, S.-Y. Xu, and N. Ni, Phys. Rev. B **95**, 245113 (2017).
[13] Q. Chen, Z. Lou, S. Zhang, B. Xu, Y. Zhou, H. Chen, S. Chen, J. Du, H. Wang, J. Yang, Q. Wu, O. V. Yazyev, and M. Fang, Phys. Rev. B **102**, 165133 (2020).
[14] D. Pesin and L. Balents, Nature Physics **6**, 376 (2010).
[15] M. Dzero, K. Sun, V. Galitski, and P. Coleman, Phys. Rev. Lett. **104**, 106408 (2010).
[16] M. Dzero, K. Sun, P. Coleman, and V. Galitski, Phys. Rev. B **85**, 045130 (2012).
[17] F. Lu, J. Zhao, H. Weng, Z. Fang, and X. Dai, Phys. Rev. Lett. **110**, 096401 (2013).
[18] X.-L. Qi and S.-C. Zhang, Rev. Mod. Phys. **83**, 1057 (2011).
[19] D. N. Sheng, Z. C. Gu, K. Sun, and L. Sheng, Nature Communications **2**, 389 (2011).
[20] N. Regnault and B. A. Bernevig, Phys. Rev. X **1**, 021014 (2011).
[21] T. Neupert, L. Santos, C. Chamon, and C. Mudry, Phys. Rev. Lett. **106**, 236804 (2011).
[22] S. Wolgast, i. m. c. b. u. i. e. i. f. Kurdak, K. Sun, J. W. Allen, D.-J. Kim, and Z. Fisk, Phys. Rev. B **88**, 180405 (2013).
[23] D. Kim, S. Thomas, T. Grant, J. Botimer, Z. Fisk, and J. Xia, Scientific reports **3**, 3150 (2013).
[24] G. Li, Z. Xiang, F. Yu, T. Asaba, B. Lawson, P. Cai, C. Tinsman, A. Berkley, S. Wolgast, and Y. S. a. Eo, Science **346**, 1208 (2014).
[25] S. Thomas, D. J. Kim, S. B. Chung, T. Grant, Z. Fisk, and J. Xia, Phys. Rev. B **94**, 205114 (2016).
[26] N. Xu, X. Shi, P. K. Biswas, C. E. Matt, R. S. Dhaka, Y. Huang, N. C. Plumb, M. Radović, J. H. Dil, E. Pomjakushina, K. Conder, A. Amato, Z. Salman, D. M. Paul, J. Mesot, H. Ding, and M. Shi, Phys. Rev. B **88**, 121102 (2013).
[27] J. Jiang, S. Li, T. Zhang, Z. Sun, F. Chen, Z. R. Ye, M. Xu, Q. Q. Ge, S. Y. Tan, and X. H. a. Niu, Nature Communications **4**, 3010 (2013).
[28] J. D. Denlinger, J. W. Allen, J.-S. Kang, K. Sun, B.-I. Min, D.-J. Kim, and Z. Fisk, in *Proceedings of the International Conference on Strongly Correlated Electron Systems (SCES2013)* (2014) p. 017038.
[29] M. M. Yee, Y. He, A. Soumyanarayanan, D.-J. Kim, Z. Fisk, and J. E. Hoffman, arXiv preprint arXiv:1308.1085 (2013).
[30] N. M. Q. S. Wu, G. Autès and O. V. Yazyev, Materials Cloud Archive 2019.0019/v2 (2019), 10.24435/materialscloud:2019.0019/v2.
[31] M. Vergniory, L. Elcoro, C. Felser, N. Regnault, B. A. Bernevig, and Z. Wang, Nature **566**, 480 (2019).
[32] T. Zhang, Y. Jiang, Z. Song, H. Huang, Y. He, Z. Fang, H. Weng, and C. Fang, Nature **566**, 475 (2019).
[33] F. Tang, H. C. Po, A. Vishwanath, and X. Wan, Nature **566**, 486 (2019).
[34] C. Xu, J. Chen, G.-X. Zhi, Y. Li, J. Dai, and C. Cao, Phys. Rev. B **93**, 195106 (2016).
[35] B. Shen, X. Deng, G. Kotliar, and N. Ni, Phys. Rev. B **93**, 195119 (2016).
[36] D. Wu, J. Liao, W. Yi, X. Wang, P. Li, H. Weng, Y. Shi, Y. Li, J. Luo, X. Dai, and Z. Fang, Appl. Phys. Lett. **108**, 042105 (2016).
[37] Y.-Y. Wang, Q.-H. Yu, P.-J. Guo, K. Liu, and T.-L. Xia, Phys. Rev. B **94**, 041103 (2016).
[38] Y. Li, L. Li, J. Wang, T. Wang, X. Xu, C. Xi, C. Cao, and J. Dai, Phys. Rev. B **94**, 121115 (2016).
[39] Z. Yuan, H. Lu, Y. Liu, J. Wang, and S. Jia, Phys. Rev. B **93**, 184405 (2016).
[40] Y. Luo, R. D. McDonald, P. F. S. Rosa, B. Scott, N. Wakeham, N. J. Ghimire, E. D. Bauer, J. D. Thompson, and F. Ronning, Sci. Rep. **6**, 27294 (2016).
[41] B. Wang, B. Singh, B. Ghosh, W.-C. Chiu, M. M. Hosen, Q. Zhang, L. Ying, M. Neupane, A. Agarwal, H. Lin, and A. Bansil, Phys. Rev. B **100**, 205118 (2019).
[42] Z. Wang, Y. Zheng, Z. Shen, Y. Lu, H. Fang, F. Sheng, Y. Zhou, X. Yang, Y. Li, C. Feng, and Z.-A. Xu, Phys. Rev. B **93**, 121112 (2016).
[43] Y. Sun, S.-C. Wu, and B. Yan, Phys. Rev. B **92**, 115428 (2015).
[44] C.-C. Lee, S.-Y. Xu, S.-M. Huang, D. S. Sanchez, I. Belopolski, G. Chang, G. Bian, N. Alidoust, H. Zheng, M. Neupane, B. Wang, A. Bansil, M. Z. Hasan, and H. Lin, Phys. Rev. B **92**, 235104 (2015).
[45] N. J. Ghimire, Y. Luo, M. Neupane, D. J. Williams, E. D. Bauer, and F. Ronning, Journal of Physics: Condensed Matter **27**, 152201 (2015).
[46] J. Hu, J. Liu, D. Graf, S. Radmanesh, D. Adams, A. Chuang, Y. Wang, I. Chiorescu, J. Wei, L. Spinu, *et al.*, Scientific Reports **6**, 18674 (2016).
[47] S.-Y. Xu, I. Belopolski, N. Alidoust, M. Neupane, G. Bian, C. Zhang, R. Sankar, G. Chang, Z. Yuan, C.-C. Lee, S.-M. Huang, H. Zheng, J. Ma, D. S. Sanchez, B. Wang, A. Bansil, F. Chou, P. P. Shibayev, H. Lin, S. Jia, and M. Z. Hasan, Science **349**, 613 (2015).
[48] F. Hulliger, Nature **204**, 775 (1964).
[49] G. Kresse and J. Furthmüller, Phys. Rev. B **54**, 11169 (1996).
[50] G. Kresse and D. Joubert, Phys. Rev. B **59**, 1758 (1999).
[51] J. P. Perdew, K. Burke, and M. Ernzerhof, Phys. Rev. Lett. **78**, 1396 (1997).
[52] Q. Wu, S. Zhang, H.-F. Song, M. Troyer, and A. A. Soluyanov, Computer Physics Communications **224**, 405 (2018).
[53] A. A. Mostofi, J. R. Yates, G. Pizzi, Y.-S. Lee, I. Souza, D. Vanderbilt, and N. Marzari, Computer Physics Communications **185**, 2309 (2014).
[54] J. Kästner and E. Wassermann, Journal of Low Temperature Physics **29**, 411 (1977).
[55] V. K. C. Liang and C. C. Tsuei, Phys. Rev. B **7**, 3215 (1973).
[56] S. Barua, M. C. Hatnean, M. Lees, and G. Balakrishnan, Scientific reports **7**, 1 (2017).
[57] Y. Zhao, H. Liu, J. Yan, W. An, J. Liu, X. Zhang, H. Wang, Y. Liu, H. Jiang, Q. Li, Y. Wang, X.-Z. Li, D. Mandrus, X. C. Xie, M. Pan, and J. Wang, Phys. Rev. B **92**, 041104 (2015).
[58] D. V. Khveshchenko, Phys. Rev. Lett. **87**, 206401 (2001).
[59] J. Du, Z. Lou, S. Zhang, Y. Zhou, B. Xu, Q. Chen, Y. Tang, S. Chen, H. Chen, Q. Zhu, H. Wang, J. Yang, Q. Wu, O. V. Yazyev, and M. Fang, Phys. Rev. B **97**, 245101 (2018).
[60] L. R. Thoutam, Y. L. Wang, Z. L. Xiao, S. Das, A. Luican-Mayer, R. Divan, G. W. Crabtree, and W. K. Kwok, Phys. Rev. Lett. **115**, 046602 (2015).
[61] Y. L. Wang, L. R. Thoutam, Z. L. Xiao, J. Hu, S. Das, Z. Q. Mao, J. Wei, R. Divan, A. Luican-Mayer, G. W. Crabtree, and W. K. Kwok, Phys. Rev. B **92**, 180402 (2015).

[62] J. Ziman, *Electrons and Phonons, Classics Series* (Oxford University Press, 2001).
[63] F. C. Chen, H. Y. Lv, X. Luo, W. J. Lu, Q. L. Pei, G. T. Lin, Y. Y. Han, X. B. Zhu, W. H. Song, and Y. P. Sun, Phys. Rev. B **94**, 235154 (2016).
[64] Q. Zhou, D. Rhodes, Q. R. Zhang, S. Tang, R. Schönemann, and L. Balicas, Phys. Rev. B **94**, 121101 (2016).
[65] M. N. Ali, J. Xiong, S. Flynn, J. Tao, Q. D. Gibson, L. M. Schoop, T. Liang, N. Haldolaarachchige, M. Hirschberger, N. P. Ong, *et al.*, Nature **514**, 205 (2014).
[66] M. Neupane, S.-Y. Xu, R. Sankar, N. Alidoust, G. Bian, C. Liu, I. Belopolski, T.-R. Chang, H.-T. Jeng, H. Lin, *et al.*, Nature communications **5**, 1 (2014).
[67] J. Xiong, S. K. Kushwaha, T. Liang, J. W. Krizan, M. Hirschberger, W. Wang, R. J. Cava, and N. P. Ong, Science **350**, 413 (2015).